



Contents lists available at ScienceDirect

Composite Structures

journal homepage: www.elsevier.com/locate/compstruct

Reliability-based design and optimization of adaptive marine structures

Y.L. Young^{a,*}, J.W. Baker^c, M.R. Motley^b^a Department of Naval Architecture and Marine Engineering, University of Michigan, Ann Arbor, MI 48109, USA^b Department of Civil and Environmental Engineering, Princeton University, Princeton, NJ 08544, USA^c Department of Civil and Environmental Engineering, Stanford University, Stanford, CA 94305, USA

ARTICLE INFO

Article history:

Available online 28 July 2009

Keywords:

Reliability-based design and optimization
 Adaptive marine structure
 Fluid–structure interaction
 Composite blade
 Propeller
 Turbine

ABSTRACT

The objectives of this work are to quantify the influence of material and operational uncertainties on the performance of self-adaptive marine rotors, and to develop a reliability-based design and optimization methodology for adaptive marine structures. Using a previously validated 3D fluid–structure interaction model, performance functions are obtained and used to generate characteristic response surfaces. A first-order reliability method is used to evaluate the influence of uncertainties in material and load parameters and thus optimize the design parameters. The results demonstrate the viability of the proposed reliability-based design and optimization methodology, and demonstrate that a probabilistic approach is more appropriate than a deterministic approach for the design and optimization of adaptive marine structures that rely on fluid–structure interaction for performance improvement.

© 2009 Elsevier Ltd. All rights reserved.

1. Introduction

Self-adaptive structures are those which change in shape or property via active and/or passive control mechanisms to automatically adjust to the changing environment. Active, passive, and hybrid control mechanisms have been exploited to achieve adaptive/intelligent/smart designs. Among the passive control mechanisms, one important class involves the use of fluid–structure interactions.

In aerospace engineering, utilization of fluid–structure interactions for performance enhancement has been well documented. In Khan [1], aeroelastic behaviors of composite helicopter blades were investigated to improve propeller performance, including thrust, power, and efficiency. Studies have also shown that aeroelastic tailoring and optimization of composite helicopter blades can improve stability, reduce vibration, and reduce hub and dynamic blade loads [2–6]. In Yang [7], fluid–structure interaction analysis was performed for a composite canard structure, where the possibility of achieving higher efficiency and better maneuverability was numerically demonstrated. Passive control technologies have also been considered for wind turbines, where material load–deformation coupling was used to reduce fatigue damage through load-mitigation at high winds (see Refs. Lee and Flay [8], Lobitz et al. [9]), and to improve energy capture (see Ref. Lobitz and Veers [10]).

In marine and ocean engineering, investigations into methodologies that utilize fluid–structure interactions have also been on the

rise. In Gowing et al. [11], experimental studies demonstrated that load-induced deformations of composite elliptic hydrofoils helped to delay cavitation inception, while maintaining the overall lift and drag. Numerical [12–17] and experimental [18] studies have also shown that passive pitch adjustments through the use of anisotropic laminated composites helped to increase the fuel-efficiency of marine propellers over a range of operating conditions. Similar passive pitch adjustment strategies have also been explored to increase the energy capture of marine/current turbines in Nicholls-Lee and Turnock [19].

The focus of the current work is on passive, self-adaptive marine structures that utilize fluid–structure interactions. Because the performance of these structures depends on fluid–structure interactions, they may be more sensitive to random variations in material and load uncertainties. Hence, the objective of this work is to develop a reliability-based design and optimization methodology to improve the performance and reliability of adaptive marine structures. To demonstrate the methodology, results are shown for a self-adaptive composite marine propeller, but the methodology is generally applicable to other adaptive structures that undergo fluid–structure interaction.

1.1. Reliability-based design and optimization of self-adaptive structures

Reliability-based design and optimization is a common practice for many rigid and/or non-adaptive structural engineering systems. The objective is to ensure the level of required reliability is achieved with respect to uncertainties in structural parameters and operating conditions.

* Corresponding author. Tel.: +1 734 936 7636; fax: +1 734 936 8820.

E-mail addresses: ylyoung@umich.edu, ylyoung@princeton.edu (Y.L. Young).

Although much progress in this field has been made for rigid and/or non-adaptive structures (see [20] for a recent review in this area), relatively little work focuses on flexible structures that interact with the environment. Reviews of the state-of-the-art methods in reliability-based design and optimization of aeroelastic structures can be found in [21]. As noted in [21], only limited work has been done on reliability analysis of structures undergoing fluid–structure interactions, and most existing methods employed simplistic linear fluid and fluid–structure interaction models to determine the mechanical response, which introduce epistemic modeling uncertainty. Hence, [21] introduced a reliability analysis method that integrates a coupled Euler flow solver with a structural finite element model (FEM) for the deterministic aeroelastic analysis of a 3D wing structure, and employed a first-order reliability method (FORM) to evaluate the performance sensitivities to design parameters, operating conditions, and modeling uncertainties. A probabilistic design assessment of smart composite structures is presented in [22] in which sensitivity factors were developed for a series of design parameters for a composite wing based on their effects on the angle of attack and impact response of the structure. By improving the reliability of design parameters with the highest sensitivity factors, the failure probability was reduced for the structure. The stochastic nature of composite properties has also been shown to lead to overestimation of structural reliability. By using a probabilistic design methodology, improvements can be made over traditional deterministic design methods [23]. In [24], the reliability of a thin-walled circular composite cylinder was shown to have a strong sensitivity to the applied load and to the amount of parametric scatter via multiple response surface techniques.

It should be noted that all of the above mentioned reliability-based design and optimization methods focus on adaptive/smart aerospace structures. Similar work is also needed for adaptive marine structures, where the fluid loading tends to be much higher (due to the higher fluid density and viscosity), the flow may be highly unsteady (due to transient structural motion, as well as spatial and temporal variations in the flow field), and may be susceptible to cavitation damage.

1.2. Objectives

The objectives of this work are to (1) quantify the influence of material and load uncertainties on the performance of self-adaptive marine structures and (2) optimize the design to achieve the desired level of reliability in structural performance and, in doing so, develop a reliability-based design and optimization method for adaptive marine structures.

2. Self-adaptive composite marine propellers

Marine propellers are traditionally made of nickel–aluminum–bronze (NAB) due to its excellent stiffness, yield strength, and anti-biofouling characteristics. They are designed to be rigid, and the blade geometry is optimized to yield the maximum efficiency at the design flow condition. However, when the advance speed or the shaft rotational frequency moves away from the design values, the blade geometry becomes sub-optimal relative to the changed inflow, and hence leads to decreases in energy efficiency. The effect is more severe when a rigid propeller is operating behind an asymmetric wake (caused by interactions with the upstream hull, inclined shaft, ship maneuvering, etc.) because the resultant inflow angle will vary periodically with blade position. Consequently, the efficiency of a rigid propeller tends to decrease when operating behind spatially varying wake. This problem can be minimized by using blades made of carbon fiber reinforced plastics

(CFRP). In addition to the well-known higher specific stiffness and higher specific strength of CFRP, the intrinsic deformation coupling behavior of anisotropic composites can be utilized to improve the propeller performance by passive tailoring of the load-induced deformations according to the changing inflow, as demonstrated in recent numerical (see Lee and Lin [12], Lin and Lee [13], Young et al. [14], Young and Liu [15], Young [16], Motley et al. [17]) and experimental (see Chen et al. [18]) studies. Nevertheless, all of the work thus far on self-adaptive composite marine propellers has been limited to deterministic analysis. Since the performance of these structures is more sensitive to material or load uncertainties due to their dependence on fluid–structure interaction, a reliability-based design and optimization method that can consider natural or man-made variations is needed.

3. Problem definition

To perform a reliability-based evaluation of the structure, we will need to evaluate two performance measures. First, we must find the probability of unsatisfactory performance. This is done by defining a limit state function, $g(\mathbf{X})$, where \mathbf{X} consists of a vector of design variables, \mathbf{X}_D , either deterministic or random, and a vector of random variables, \mathbf{X}_R , representing uncertain structural properties and loading conditions, and $g(\cdot)$ is a function that relates the design variables, random variables and the performance of the structure. The function $g(\mathbf{X})$ can either be implicit (e.g., the outcome of a numerical BEM–FEM code), or explicit (e.g., an approximate equation obtained using the response surface method). The function $g(\mathbf{X})$ is chosen such that $g(\mathbf{X}) = 0$ defines a boundary between satisfactory and unsatisfactory performance (with $g(\mathbf{X}) < 0$ indicating that the structure has unacceptable performance, and $g(\mathbf{X}) > 0$ indicating acceptable performance). The performance state associated with the boundary $g(\mathbf{X}) = 0$ is denoted as a “limit state”. Given this formulation, the optimization problem herein can be written as

$$\max_{\mathbf{X}_D} [p(g_{obj}(\mathbf{X}) > 0)] \quad (1)$$

$$\text{or } \min_{\mathbf{X}_D} [p(g_{obj}(\mathbf{X}) \leq 0)]$$

where $g_{obj}(\mathbf{X})$ is the objective function, based on the efficiency (η) of the adaptive composite propeller, which is required to be greater than a minimum target efficiency for all loading conditions, ϵ_η :

$$g_{obj}(\mathbf{X}) = \eta(\mathbf{X}) - \epsilon_\eta \quad (2)$$

subject to two probabilistic limit state functions g_1^{prob} and g_2^{prob} .

$$g_j^{prob} = p_{fj} - p(g_{fj}(\mathbf{X}) < 0) \geq 0; \quad j = 1, 2 \quad (3)$$

where the constraint functions g_{fj} are defined as

$$g_{f1}(\mathbf{X}) = 1 - \frac{P_{ST}(\mathbf{X})}{P_{rigid}(J)} \quad (4)$$

$$g_{f2}(\mathbf{X}) = \frac{\Delta_{max}}{D} - \frac{\Delta(\mathbf{X})}{D} \quad (5)$$

subject to an acceptable probability of failure, $\mathbf{p}_f = [p_{f1} \ p_{f2}]^T$. We denote $\eta(\mathbf{X})$ as the efficiency of the self-twisting propeller. $P_{ST}(\mathbf{X})$ and $P_{rigid}(J)$ represent the power demand of the self-twisting and rigid propellers, respectively. Note here that the performance of the rigid propeller is a function of the loading condition represented by the advance coefficient $J = V/nD$ (ratio of mean relative inflow velocity to rotor tip velocity) only because the objective is to optimize the design variables for the self-twisting propeller such that it yields equal or better performance compared to the already optimized rigid propeller. The rigid propeller is only used as a reference to evaluate the performance of the adaptive propeller. It should be noted here that V is the propeller advance speed, D is the propeller diameter, and n is the propeller rotational frequency.

In the application considered here, the vector of random variables is defined as $\mathbf{X}_R = [J, E_1, E_2, G_{12}, \nu_{12}, \nu_{21}]^T$. For the sake of simplicity, the blades are assumed to be made of a single layer of orthotropic lamina with material properties $E_1, E_2, G_{12}, \nu_{12}$, and ν_{21} and the fibers are oriented at angle θ counterclockwise relative to the local spanwise direction. Again for simplicity, the only design variable considered is the fiber orientation angle, $\mathbf{X}_D = \theta$. The objective of the optimization problem is to find the best fiber orientation angle, θ , that maximizes the overall efficiency of the self-twisting propeller, as represented by Eq. (2), subject to design constraints represented by Eqs. (4) and (5).

Eq. (4) is used to ensure that the expected average power demand of the self-twisting propeller is less than that of the rigid propeller, which will guarantee that the self-twisting propeller provides higher averaged energy efficiency. Further, we define $\frac{\Delta(\mathbf{x})}{D}$ as the blade tip deflection (Δ) normalized by the propeller diameter (D), a parameter which is limited by the maximum allowable normalized blade tip deflection ($\frac{\Delta_{max}}{D}$). The blade tip deflection needs to be restrained to limit the possibility of blade strength and stiffness failures. It should be noted that composite blades made of CFRP can have many possible material failure modes, as well as hydroelastic instability failure modes, most of which can be correlated to the tip deflections. As such, the tip deflection, Eq. (5), defines the safety limit to ensure structural stability and integrity. Eq. (4) is used to represent the serviceability limit because its objective is to minimize power demand. Eqs. (4) and (5) limit the optimal design range and the objective function (Eq. (2)) is used to find the fiber orientation angle that maximizes the probability of exceeding the minimum target energy efficiency of the self-twisting propeller.

4. Fluid–structure interaction analysis method

The numerical modeling involves a deformable composite propeller subjected to a spatially varying inflow wake \mathbf{V}_E . The model has been validated against analytical, numerical, and experimental results [14,25,15,16].

The governing equation for the fluid is the incompressible Euler equation in a blade-fixed rotating coordinate system:

$$\begin{aligned} D\mathbf{V}_t/Dt &= -\nabla p/\rho + \mathbf{g} - \boldsymbol{\Omega} \times (\boldsymbol{\Omega} \times \mathbf{x}) - 2\boldsymbol{\Omega} \times \mathbf{V}_t \\ \nabla \cdot \mathbf{V}_t &= 0 \end{aligned} \quad (6)$$

where \mathbf{V}_t is the total velocity, t is the physical time, p is the hydrodynamic pressure, ρ is the water density, \mathbf{g} is the gravitational acceleration, and $\boldsymbol{\Omega}$ is the propeller rotational speed vector. The total velocity (\mathbf{V}_t) can be expressed as the sum of the inflow velocity (\mathbf{V}_{in}) and a perturbation potential velocity ($\nabla\phi$) where the inflow velocity can be decomposed into the effective wake velocity (\mathbf{V}_e) and the blade rotational velocity: $\mathbf{V}_{in} = \mathbf{V}_e - \boldsymbol{\Omega} \times \mathbf{x}$. The effective wake velocity \mathbf{V}_e is obtained either from experimental measurements [26] or from a coupled RANS/Euler and potential flow solver [27]. It includes the interaction between the nominal wake vorticity (in the absence of the propeller) and the vorticity induced by the propeller [27]. The perturbation flow field can be treated as incompressible, inviscid, and irrotational. Hence, it satisfies the Laplace equation: $\nabla^2\phi = 0$. Further, the perturbation potential ϕ can be decomposed into two parts, namely, ϕ , which is due to rigid blade rotation, and φ , which is due to elastic blade deformation. Both ϕ and φ can be formulated as a mixed boundary value problem in the time-domain and solved using a 3D boundary element method (BEM) [25,16].

By virtue of the previous decomposition, the finite element discretization for structural analysis in the rotating blade-fixed coordinate system can be formulated as follows:

$$\begin{aligned} ([\mathbf{M}] + [\mathbf{M}_H])\{\ddot{\mathbf{u}}\} + ([\mathbf{C}] + [\mathbf{C}_H])\{\dot{\mathbf{u}}\} + [\mathbf{K}]\{\mathbf{u}\} \\ = \{\mathbf{F}_{ce}\} + \{\mathbf{F}_{co}\} + \{\mathbf{F}_r\} \end{aligned} \quad (7)$$

where $\{\ddot{\mathbf{u}}\}$, $\{\dot{\mathbf{u}}\}$, and $\{\mathbf{u}\}$ are the structural nodal acceleration, velocity, and displacement vectors, respectively; $[\mathbf{M}]$, $[\mathbf{C}]$, and $[\mathbf{K}]$ are the structural mass, damping, and stiffness matrices, respectively; $[\mathbf{M}_H]$ and $[\mathbf{C}_H]$ are called the hydrodynamic added mass and hydrodynamic damping matrices, respectively, because $[\mathbf{M}_H]$ is associated with $\{\ddot{\mathbf{u}}\}$ and $[\mathbf{C}_H]$ is associated with $\{\dot{\mathbf{u}}\}$. Notice that $\{\mathbf{F}_v\} = -[\mathbf{M}_H]\{\ddot{\mathbf{u}}\} - [\mathbf{C}_H]\{\dot{\mathbf{u}}\}$ represents the dynamic hydroelastic force caused by fluid–structure interaction, and can be derived by application of the pressure and velocity compatibility conditions at the blade surface [25,16]. $\{\mathbf{F}_{ce}\}$, $\{\mathbf{F}_{co}\}$, and $\{\mathbf{F}_r\}$ are the centrifugal force, the Coriolis force, and the hydrodynamic force (due to rigid blades rotation) vectors, respectively. Detailed formulation of these matrix identities can be found in [25,16]. Eq. (7) can be solved using standard finite element methods (FEM) in the time-domain such as ABAQUS/Standard [28]. User-developed subroutines are utilized to superimpose the hydrodynamic added mass matrix $[\mathbf{M}_H]$ with the structural mass matrix $[\mathbf{M}]$, and the hydrodynamic damping matrix $[\mathbf{C}_H]$ with the structural damping matrix $[\mathbf{C}]$, and to perform iterations between the BEM and FEM solvers to consider nonlinear FSI effects induced by large blade deformations.

5. Problem setup

The propeller herein is modeled using a single layer for simplicity, but the actual model will have many layers and will be stacked in a sequence such that the load–deformation characteristics will be the same as the effective single layer model [29]. However, it should be cautioned that such simplification is only appropriate to determine the load–deformation characteristics for linear-elastic structural systems. Detailed stress analysis using the actual multi-layer model should be performed after the hydroelastic optimization analysis to verify structural integrity.

The material selected is Hexcel IM7-8552 carbon epoxy composite. The mean-load geometry is based on that of propeller 5474 (Fig. 1), one of the composite propellers manufactured by AIR Fertigung-Technologie GmbH and designed and tested in cooperation with the Naval Surface Warfare Center, Carderock Division (NSWCCD). The propeller has a diameter of $D = 0.6096$ m. The design rotational frequency is $n = 780$ rpm. The design advance coefficient is $J = V/nD = 0.66$. More details of propeller 5474 can be found in [18,15].

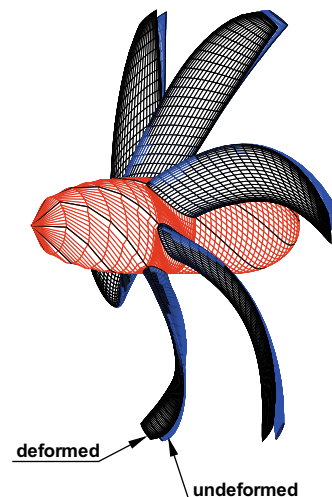


Fig. 1. Deformed and undeformed geometry of the self-twisting propeller.

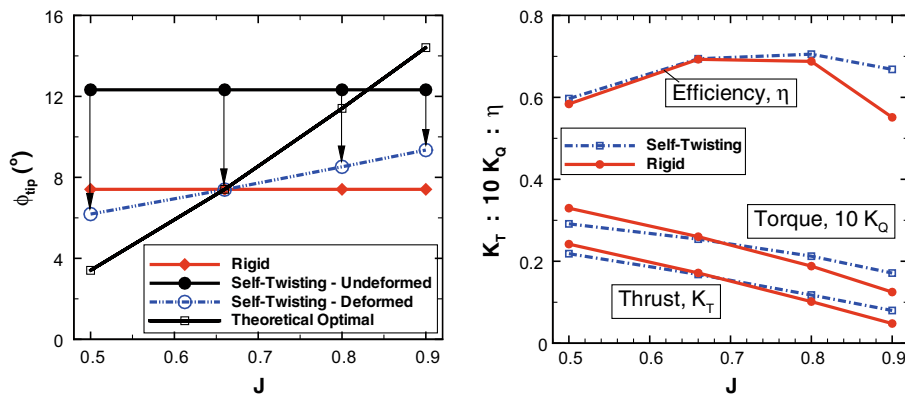


Fig. 2. Comparison of the tip pitch angle (left) and performance curves (right) for the rigid and self-twisting propellers.

Fig. 2 compares the performance of the adaptive self-twisting propeller with its rigid counterpart based on deterministic fluid–structure interaction analysis using the method outlined in Section 4. As shown in the left plot, the adaptable propeller geometry (represented by the tip pitch angle, ϕ_{tip}) approaches the theoretical optimal propeller geometry, which changes with the advance coefficient (J is inversely proportional to the angle of attack). For the possible range of J values for forward operations, the self-twisting propeller is designed to be overpitched in its unloaded (undeformed) configuration. The self-twisting propeller de-pitches due to twisting motion induced by bending deformation caused by the fluid loading, which changes with J (operating condition). The design requirements are that:

1. At $J = J_{design} = 0.66$, the deformed geometry of the self-twisting propeller matches the optimized rigid propeller geometry to achieve equivalent performance between the two propellers.
2. At all $J \neq J_{design}$, the self-twisting propeller should yield higher energy efficiency than its rigid counterpart.

The efficiency is defined as $\eta = TV/2\pi nQ = JK_T/(2\pi K_Q)$ which corresponds to the ratio of the thrust power to the available shaft power, with thrust coefficient $K_T = T/\rho n^2 D^4$ and torque coefficient $K_Q = Q/\rho n^2 D^5$. T and Q are the dimensional thrust and torque, respectively. As shown in Fig. 2, the rigid and the self-twisting propellers exhibit similar performance at the design condition $J = 0.66$. The efficiency of the self-twisting propeller is higher than its rigid counterpart for all $J \neq 0.66$. The efficiency improvement increases as the flow condition further deviates from the design condition. Further, the resulting thrust and torque exhibit smoother variation with changing J . The result is a propeller that is, on average, more energy efficient than its rigid counterpart, requiring less power to operate and less variation in power, which reduces the strain and extends the fatigue life of the engine. For details about the design procedure or fluid–structure interaction analysis methodology, readers should refer to [14,30,16,17].

6. Parametric sensitivity for R

To further simplify the model, parametric sensitivity analyses of the random variables \mathbf{X}_R were performed (see Figs. 3 and 4). By taking each of the material parameters and providing them with a normal distribution (i.e. with mean $\mu(\mathbf{X}_R) = \mathbf{X}_{R,design} = [J, E_1, E_2, G_{12}, \nu_{12}, \nu_{21}] = [0.66, 171.42 \text{ GPa}, 9.08 \text{ GPa}, 5.29 \text{ GPa}, 0.32, 0.32]$ and standard deviation $\sigma(\mathbf{X}_R) = 0.02\mu(\mathbf{X}_R)$ based on expected tolerances, the sensitivities to these variables can be assessed. The material parameters were assigned extreme deviations from the design values of three standard deviations (99.7% of the

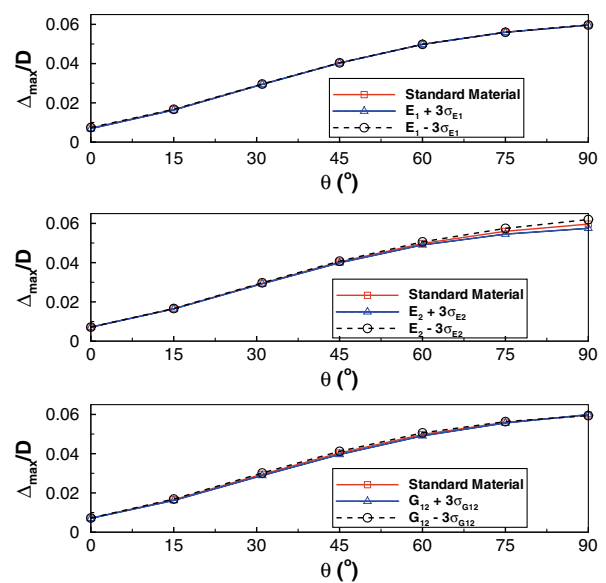


Fig. 3. Effect of variations in material properties on the blade tip deflection for the self-twisting propeller.

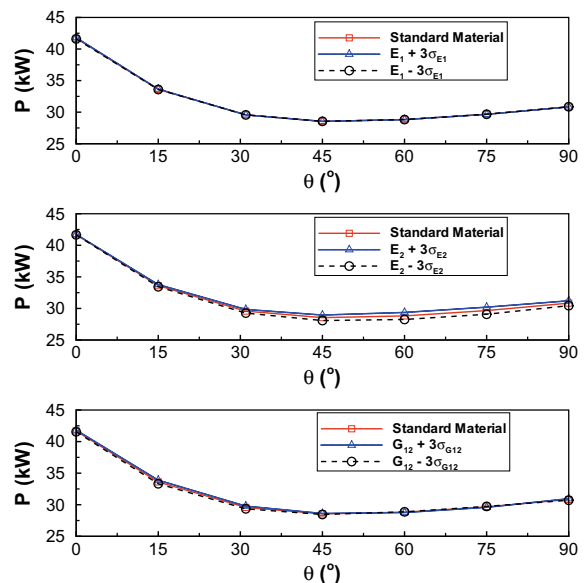


Fig. 4. Effect of variations in material properties on the power requirement for the self-twisting propeller.

realizations of a normal distribution are within three standard deviations of the distribution mean), and compared with the design condition (i.e. $\mathbf{X}_{R,design}$).

As shown in Figs. 3 and 4, the effects of variations in the primary bending modulus (E_1) and shear modulus (G_{12}) are negligible. Bounds for extreme values of the secondary bending modulus (E_2), however, noticeably deviate from the design behavior, particularly for large θ . This is because at low values of θ , the primary stiffness is governed by $E_1 = 171.42$ GPa, which is a much larger value compared to $E_2 = 9.08$ GPa. Hence, even at three standard deviations from the mean (161.13 GPa $\leq E_1 \leq 181.71$ GPa), the effects on the normalized bending deflection and power are small due to the high stiffness. On the other hand, as θ approaches 90° , the primary bending stiffness of the blade is governed by (E_2). Because E_2 is comparatively small with respect to E_1 , the system behavioral effects for variations in E_2 are magnified, though only marginally. For the purposes of this paper, however, it is assumed that the material parameters, except for θ , have negligible effect on the efficiency, power requirement, and tip displacement of the propeller blades. As such, the random variable vector \mathbf{X}_R can be simplified to only contain the advance coefficient, J .

7. Response surface methodology

The fully-coupled boundary element method-finite element method (BEM-FEM) model [25,16] summarized in Section 4 is used for the design and analysis of adaptive composite marine rotors. Although the coupled BEM-FEM analysis method is relatively fast, it can still be computationally expensive to use, with wait time requirements ranging from 5 min to 2 h for a single simulation on a single processor depending on if the analysis is steady, unsteady, with or without cavitation. For a Monte Carlo analysis large enough to successfully achieve a reliable optimization, this becomes impractical. Since the behavior of the performance (power, deflection, and efficiency) is expected to be smooth functions of J and θ , the response surface methodology is a reasonable analysis alternative. Data points obtained from the BEM-FEM model were used to predict the behavior of the self-twisting composite propeller. By using a fully two-dimensional regression analysis, equations for the response surface of the self-twisting propeller power requirement, tip deflection, and efficiency were developed:

$$P_{ST}(J, \theta) = 10^4 W (5.818 - 0.104J - 0.0909\theta + 0.0516J\theta - 4.020J^2 + 0.000772\theta^2 + 0.000361J\theta^2 - 0.0304J^2\theta - 0.000330J^2\theta^2) \quad (8)$$

$$\frac{A(J, \theta)}{D} = 0.0060 - 0.0010J + 0.0019\theta - 0.0013J\theta - 0.0021J^2 - 0.000006\theta^2 + 0.000005J\theta^2 - 0.00031J^2\theta - 0.000001J^2\theta^2 \quad (9)$$

$$\eta(J, \theta) = -0.2358 + 2.2626J + 0.0015\theta + 0.0058J\theta - 1.3411J^2 - 0.0001J\theta^2 - 0.0105J^2\theta + 0.0001J^2\theta^2 \quad (10)$$

where J is dimensionless, θ is in degrees, and W represents units of watts for the power surface. The goodness-of-fit of the surfaces can be represented by the coefficients of determination for the power demand, blade tip deflection, and efficiency, which are 0.997, 0.997, and 0.988, respectively, where

$$R^2 = 1 - \frac{\sum (g_{BEM-FEM} - \bar{g}_{BEM-FEM})^2}{\sum (g_{BEM-FEM} - g(\mathbf{X}))^2} \quad (11)$$

where $g_{BEM-FEM}$ is the data obtained from the numerical BEM-FEM model, $\bar{g}_{BEM-FEM}$ is the mean of all data obtained from the BEM-

FEM model, and $g(\mathbf{X})$ is the data generated from the response surface method; R^2 values closer to 1.0 represent higher accuracy.

The contour maps of the fitted response surfaces and data computed using the BEM-FEM numerical solver are shown in Figs. 5–7. The shaded contour values represent the fitted equations, while the dashed contour lines represent the BEM-FEM simulation data.

The power requirement is more sensitive to J than to θ . Lower values of J correspond to higher angles of attack and higher loads and thereby higher power demands. At higher loads, the change in pitch caused by the fluid-structure interaction is also greater, and hence the power demand is more sensitive to θ at lower J values. At high J values, the power demand is lower and is less sensitive to θ due to small changes in pitch caused by the hydrodynamic load induced bending-twisting deformation.

The maximum deflection is a strong function of both J and θ . This is because, as the fiber orientation angle becomes larger, the blades are less stiff along their primary (longitudinal) axis (which, at $\theta = 45^\circ$ becomes oriented more as the secondary axis). As a result, the blade tip deflections have nonlinear growth with fiber orientation angle. The increasing of the tip deflection with decreasing J is also expected due to increasing longitudinal load.

The efficiency is highest near the design values ($J = J_{design} = 0.66$, $\theta = \theta_{design} = 32^\circ$), which means that the original design

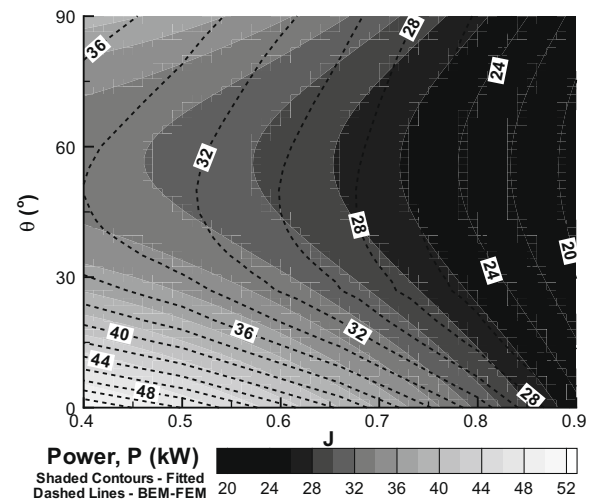


Fig. 5. Power demand, P (kW), contour map for the self-twisting propeller.

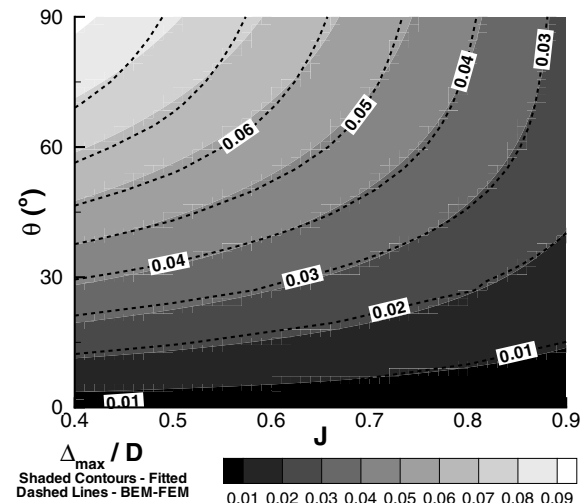


Fig. 6. Normalized blade tip deflection, Δ_{max}/D , contour map for the self-twisting propeller.

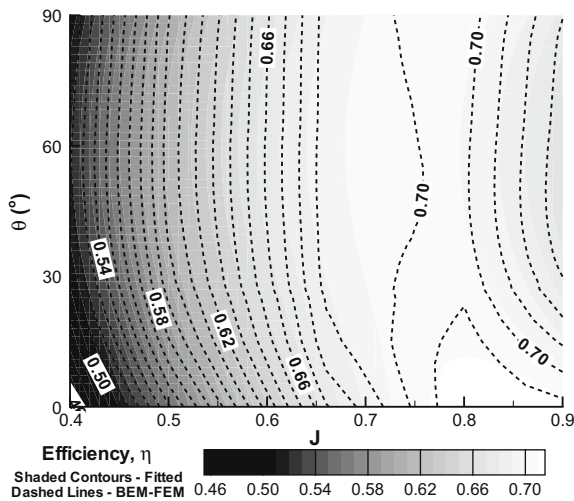


Fig. 7. Propeller efficiency, η , contour map for the self-twisting propeller.

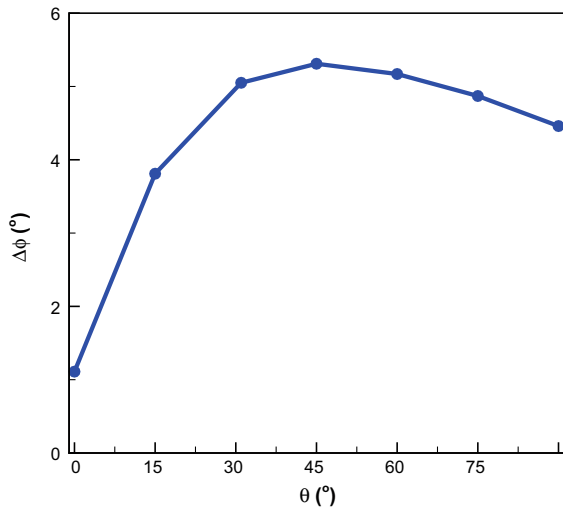


Fig. 8. Change in tip pitch angle with fiber orientation angle for the self-twisting propeller at $J = J_{design}$.

objectives are satisfied. Note that the efficiency of the adaptive composite propeller has a strong dependence on J , which is inversely proportional to the angle of attack, but a weaker dependence on θ . It is of note, however, that there exists a quadratic element to the behavior of the surface based on the fiber orientation angle. This curvature switches directions at $J = 0.66$ and the local maximum and minimum point is located at $\theta = \theta_{design}$, a characteristic which the response surface takes into account. This change in curvature can be explained by combining the behavior shown in Figs. 8 and 2. According to Fig. 8, for $\theta > 32^\circ$ and $\theta < 32^\circ$, the change in tip pitch angle, $\Delta\phi$, will be less than $\Delta\phi|_{\theta=\theta_{design}=32^\circ}$. According to Fig. 2, for $J < J_{design} = 0.66$, if $\Delta\phi < \Delta\phi|_{\theta_{design}}$, the loaded pitch distribution will be further away from the theoretical optimal value and hence $\eta < \eta|_{\theta_{design}}$; for $J > J_{design} = 0.66$, if $\Delta\phi < \Delta\phi|_{\theta_{design}}$, the loaded pitch distribution will be closer to the theoretical optimal value and hence $\eta > \eta|_{\theta_{design}}$.

The rigid propeller power requirement does not require response surface methodology as it is only a function of J ; however, fitting a curve to define the behavior of the rigid propeller is also faster than using the BEM model to compute the behavior at each J value (FEM analysis is not necessary since the blades are assumed

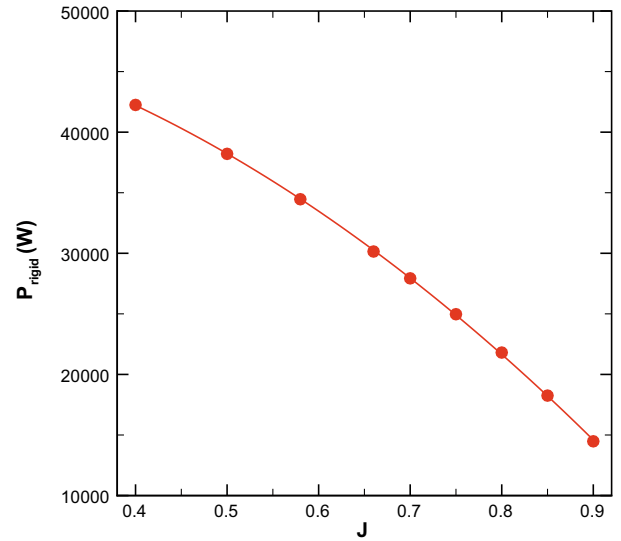


Fig. 9. Polynomial curve-fit for rigid propeller power requirement as a function of J .

to be rigid). Using polynomial fitting techniques, a second-order curve was used to fit the data ($R^2 = 0.999$) for the rigid propeller (Fig. 9):

$$P_{rigid}(J) = 10^4 W(-38572J^2 - 5091J + 50416) \quad (12)$$

8. First-order reliability method

Eq. (1) defines the probability of unacceptable performance, and computing this probability requires integration of the probability density function of \mathbf{X} over the domain of \mathbf{x} values that would result in unacceptable performance

$$p_f = p(g(\mathbf{X}) < 0) = \int_{g(\mathbf{x}) \leq 0} f_{\mathbf{X}}(\mathbf{x}) d\mathbf{x} \quad (13)$$

This integral in general involves a complex high-dimensional failure domain and often cannot be performed analytically, as is the case here. Thus, we turn to the first-order reliability method (FORM), which facilitates an approximate solution of the integral by transforming the random variables \mathbf{X} into variables having a multivariate standard normal density function, linearizing the limit state function in this transformed domain, and then utilizing analytical solutions to the transformed and linearized problem [31].

In this application, the variables in \mathbf{X} do not necessarily have normal distributions, so we start by transforming each component of the vector \mathbf{X} , denoted X_i , to a corresponding standard normal variable, denoted U_i . This transformation is performed by equating the probability of non-exceedance of any numerical values of X_i and U_i . This can be stated as follows:

$$\Phi(u_i) = F_{X_i}(x_i) \quad (14)$$

where Φ is the standard normal cumulative distribution function (CDF) and F_{X_i} is the CDF of the non-normal random variable X_i . If the components of \mathbf{X} are not mutually independent, a generalization of Eq. (14) to use a Nataf or Rosenblatt transformation would be needed to remove that dependence from U . But the calculations here use only mutually independent random variables, so this component-by-component transformation is sufficient.

The nonlinear limit state functions $g(\mathbf{X})$ can be transformed into a linear limit state space $h(\mathbf{U})$ using this same transformation. We

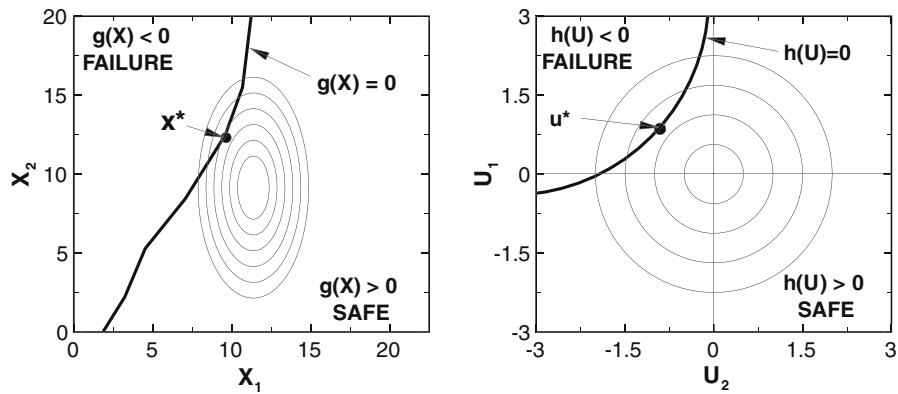


Fig. 10. Generalization of the transformation from the original \mathbf{X} space (Left) into the \mathbf{U} space (Right).

then proceed by taking advantage of the fact that $p_f = p(g(\mathbf{X}) \leq 0) = p(h(\mathbf{U}) \leq 0)$:

$$p_f = \int_{g(\mathbf{X}) \leq 0} f_{\mathbf{X}}(\mathbf{x}) d\mathbf{x} = \int_{h(\mathbf{U}) \leq 0} f_{\mathbf{U}}(\mathbf{u}) d\mathbf{u} \quad (15)$$

This mapping of the problem from \mathbf{X} -space to \mathbf{U} -space is illustrated in Fig. 10. The latter integral can still not be solved analytically, unless the limit state function $h(\mathbf{U})$ is linear. We thus linearize $h(\mathbf{U})$ at the so-called design point \mathbf{u}^* , defined as follows:

$$\mathbf{u}^* = \arg \min(\|\mathbf{U}\| \mid h(\mathbf{U}) = 0) \quad (16)$$

By this definition, \mathbf{u}^* is the point on the limit state surface $h(\mathbf{U}) = 0$ closest to the origin in \mathbf{U} -space, and thus has the highest probability density of all points in the failure domain $h(\mathbf{U}) \leq 0$. This high probability content means that linearizations of $h(\mathbf{U})$ around \mathbf{u}^* should produce p_f estimates close to the p_f estimates obtained without this linearization. Once \mathbf{u}^* is known and the limit state surface is linearized at this point, the reliability index β can be computed as

$$\beta = \alpha \mathbf{u}^* \quad (17)$$

where α is the unit normal vector perpendicular to the limit state surface at \mathbf{u}^* and pointing into the failure domain

$$\alpha = -\frac{\nabla h(\mathbf{u}^*)}{\|\nabla h(\mathbf{u}^*)\|} \quad (18)$$

This reliability index is directly related to the probability of failure by the equation

$$p_f = \Phi(-\beta) \quad (19)$$

This p_f is the FORM approximation of the p_f associated with the original non-normal random variables and nonlinear limit state function. The variables \mathbf{u}^* , α and β are illustrated graphically in Fig. 11. Several well-studied numerical algorithms for finding these variables are available [31].

In addition to the probability of failure estimate, this FORM calculation provides several other informative outputs. The elements of the vector α provide information about the relative importance of the random variables in \mathbf{U} (and, after a simple transformation, provides the same information about the original random variables \mathbf{X}). The design point \mathbf{u}^* can also be transformed (using the inverse of the operation in Eq. (14)), to find a corresponding \mathbf{x}^* : the values of \mathbf{X} that have the highest probability of causing failure of the system of interest.

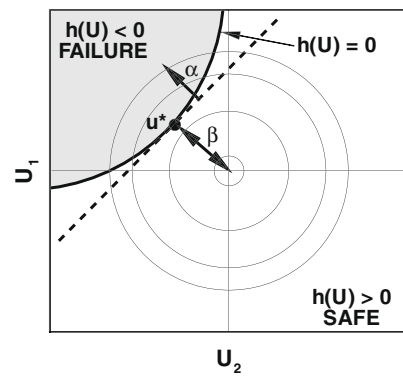


Fig. 11. Generalization of the determination of \mathbf{u}^* and β .

9. Design example

9.1. Parameter definitions

A design example is presented based on the reliability and response surface methodology explained above. The first step beyond the response surface methodology involves determining how to define the random distribution of the variables. It is typical for a manufacturer to provide a fiber orientation tolerance around $2\text{--}3^\circ$ in the construction of the laminates for propeller or turbine blades, with a confidence level of 95%. With this as a reference point, it is reasonable to assume that the fiber orientation angle has a Gaussian distribution with a mean value of θ_{design} . A tolerance of 3° with 95% confidence can be approximated by a standard deviation of 1.5° (for a normal distribution, 95% of values are within two standard deviations of the mean).

Determining an appropriate distribution for the advance coefficient is slightly less intuitive. It can be assumed that the propeller will operate near the design advance coefficient ($J_{design} = 0.66$) under most operating conditions and that this would be an appropriate mean or mode value. A standard deviation of 0.10 (for normal distribution) will provide a realistic range of operating conditions. A normal distribution, however, may not be appropriate here. Operating conditions are sensitive to many variables, including currents, waves, ship acceleration and deceleration, turning and towing. A log-normal distribution can be used to simulate a random variable that is the product of many random variables. The log-normal distribution tends more toward a positive skew (the right tail is larger). However, surface vessels tend to favor a negative skew (the left tail is larger). More often than not, deviations will occur at values lower than J_{design} because of towing or high

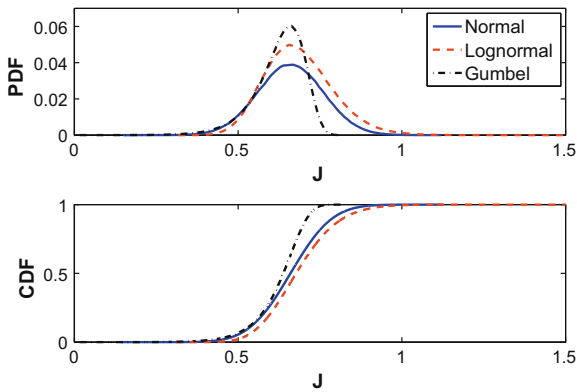


Fig. 12. Comparison of the normal, log-normal, and gumbel distribution of J .

wave resistance. As a result, the lower limit of J deviates more from the mode than the higher limit, resulting in a negative skew. This can be modeled using a Gumbel distribution, which can be generated by fixing the mode (the most frequent value) at J^{design} and limiting the minimum value to $J = 0$ (i.e. forward operations only). This ensures that the most common value, the mode, of J is that of the design condition. As shown in Fig. 12, all three distributions – shown as both a probability density function (PDF) and cumulative density function (CDF) – share the same mode, while the distribution away from the mode differs.

A second initial step is to define an acceptable maximum tip deflection and minimum target efficiency. An inherent problem of self-twisting propellers is that they can be subject to strength-based failures, as well as hydroelastic instabilities and resonance issues. As described in Section 3, by limiting the tip deflection these issues can be avoided or minimized. Hence, the value $\Delta_{max}/D = 0.05$ is selected for this design example. Extending this value too high can lead to static divergence (during deceleration and backing, although not considered here), increased stresses, and higher susceptibility to resonance. As seen in Fig. 13, $\Delta_{max}/D = 0.05$ provides a bound which limits the maximum von Mises stress to approximately 500 MPa, where the tensile and compressive fiber failure stresses for this material are 2300 and 1200 MPa, respectively. While matrix failure stresses may be an order of magnitude less than fiber failure stresses, matrix failures are generally shear based failures and the internal shear stresses tend to also be an order of magnitude smaller than the primary axis

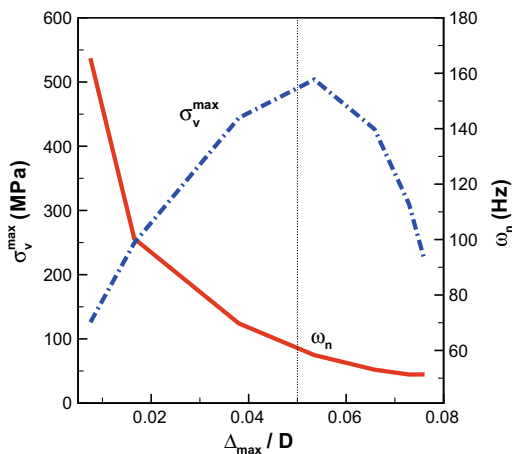


Fig. 13. Maximum von mises stress (σ_v^{max}) and fundamental frequency (ω_n) of the blade as a function of the normalized blade tip deflection, Δ_{max}/D .

stresses. Further, the natural frequency limit is approximately 60 Hz, or 3600 rpm, which is about 4.6 times higher than the design propeller rotational frequency at $n = 780$ rpm.

The minimum target efficiency for all loading conditions is set at $\epsilon_\eta = 0.60$ to ensure satisfactory performance. The serviceability limit state is set at $p_{f1} = 0.50$ to maximize the probability that the self-twisting propeller yields better performance (lower power demand), on average, than its rigid counterpart. The safety limit state is set at $p_{f2} = 0.001$ to limit the deflections to avoid strength or stability failure while allowing enough flexibility to enable performance improvement through passive bend–twist coupling induced by the hydrodynamic loads.

9.2. Validation studies

The FORM calculations of the previous section require an approximation in that they linearize the limit state surface after transforming the random variables affecting the structure performance. This linearization typically has only a minor impact on the computed failure probabilities, especially when the true failure probability is small.

To verify that FORM did not introduce any significant errors in this application, FORM and comparable Monte Carlo results are compared. Monte Carlo p_f estimates can be obtained by simulating realizations of \mathbf{X} having appropriate probability distributions, and then counting the fraction of realizations for which the structure has unacceptable performance. This approach produces p_f estimates that approach the true p_f when the number of simulations is large, because no restrictions are required on the permissible distribution of \mathbf{X} or on the form of the limit state surface. The one approximation retained here is to use the response surfaces rather than the fully coupled BEM–FEM solver to represent the structural performance. Although Monte Carlo simulations can produce estimates that converge to the true p_f value and are more widely applicable, FORM is still preferred here because of its lower computational cost and its additional diagnostic tools such as the α vector defined in Eq. (18).

Fig. 14 shows the results of the FORM methodology as compared to a 1,000,000 simulation Monte Carlo analysis based on the response surface technology described above. Note the near-

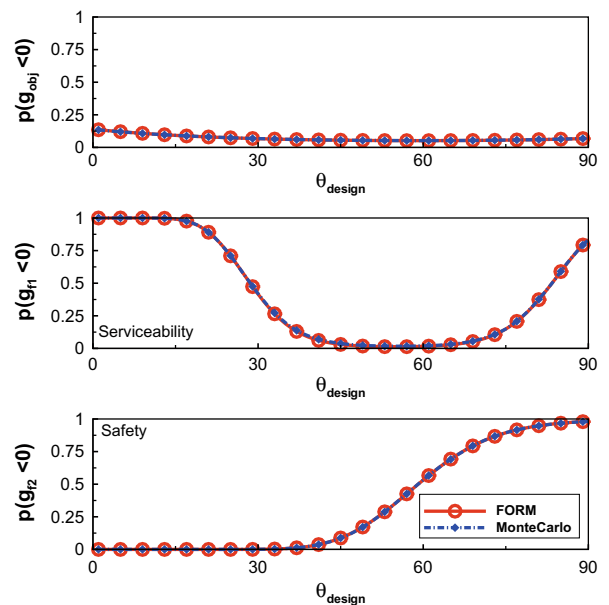


Fig. 14. FORM vs. Monte carlo methodology comparison. θ is assumed to follow a normal distribution and J is assumed to follow a gumbel distribution.

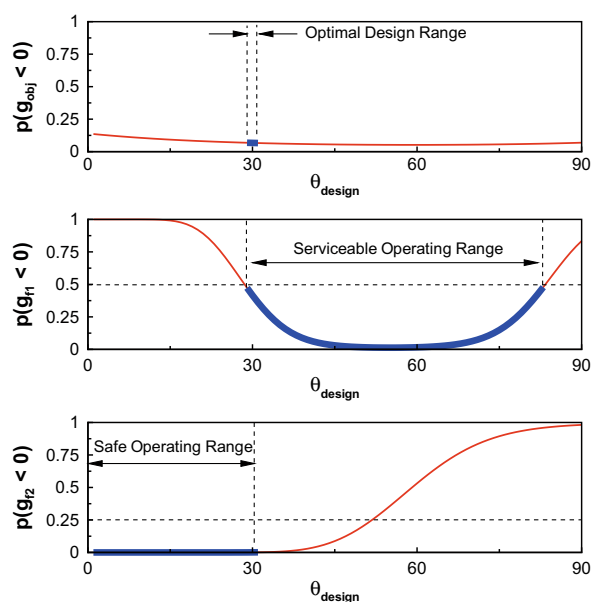


Fig. 15. Results of the FORM methodology for the probability of failure of the objective and limit state functions.

perfect agreement between the two methods, suggesting that FORM is valid for this example, where θ is assumed to follow a normal distribution and J is assumed to follow a Gumbel distribution.

9.3. Results

The results of the objective function and limit states are shown in Fig. 15. Again, θ is assumed to follow a normal distribution while J is assumed to follow a Gumbel distribution. According to the top figure, the optimal fiber orientation angle in terms of the objective function is about 59° ; however, the objective function showed little variation in the failure probability across the entire range of θ . The limit states play a very important role beyond the objective function. The constraint functions each have definitive boundaries for acceptable performance. The serviceability constraint is that the power requirement of the self-twisting propeller is, on average, lower than that of the rigid propeller, which can only be satisfied if $29^\circ \leq \theta \leq 83^\circ$. Second, the safety constraint limits the fiber orientation angle to $\theta < 31^\circ$. Hence, what seemed initially to be a wide range of viable options for the design variable based on the objective function is limited to a small range of $29^\circ \leq \theta \leq 31^\circ$. This places the optimal design based on FORM methodology to be very close to the optimal deterministic design. In this case, the probability of failure of the objective function ranges between 6.6% and 6.9%, which represents approximately 93% confidence that the self-twisting propeller will exhibit safe and improved performance over the rigid propeller for a realistic range of operating conditions.

10. Conclusions

The objective of this research is to develop a reliability-based design and optimization methodology to improve the energy efficiency of self-adapting composite marine rotors while minimizing the power requirement and susceptibility to blade failure with consideration for material and loading uncertainties. It was shown that the uncertainties in material stiffness parameters, considered as random variables, have a marginal effect on the hydroelastic behavior of the self-twisting propeller. This due to the optimization of the bending–twisting coupling that produces a system which is more sensitive to variations in θ and J than to expected

random variations in the material stiffness parameters. The distribution of the random variable J was examined with normal, log-normal, and Gumbel distributions. The Gumbel distribution was considered to be more appropriate physically, and thus was used as the advance coefficient distribution.

First-order reliability methods (FORM) were shown to be an adequate design tool instead of the more time consuming Monte Carlo simulations for probabilistic propeller optimization. Through FORM analysis, it was shown that the optimal fiber orientation angle for the adaptive propeller is $29^\circ \leq \theta \leq 31^\circ$, which will yield a 93% probability of acceptable performance based on three criteria: a serviceability limit state based on propeller power requirement, a safety limit state based on blade tip deflection, and an objective function that ensures the maximum overall energy efficiency. The serviceability limit state and constraint functions are designed such that, on average, the power requirement of the adaptive propeller is less than its rigid counterpart. The safety limit state and constraint functions are designed to limit the blade tip deflection to a specified value to prevent excessive deflections, stresses, and to reduce the susceptibility to hydroelastic instability failures. Finally, the objective function was used to determine the optimal fiber orientation angle that will maximize the average energy efficiency of the self-twisting propeller for all forward operating conditions. With the knowledge of the optimized equivalent single layer fiber orientation, a series of possible layup sequences can be developed that will provide an equivalent optimal load–deformation behavior of the blade.

The results show that a probabilistic approach is more appropriate than a deterministic approach for the design and optimization of adaptive composite structures that rely on fluid–structure interaction. This is because such structures are inherently more sensitive to random variations in material properties, geometric configurations, and loading conditions. It is important to note that, while the self-twisting propeller can be optimized for efficiency, it is possible that the limit state functions would provide no viable design option that would be both serviceable and safe. Should a design singularity occur, changes in the blade geometry, material properties, and material configurations may be necessary. Additional work is needed to assess the effect of material, geometry, and load uncertainties on the initiation and evolution of failure modes. This is more complex due to the need to consider the many layers of laminates and the many possible modes of failure, as well as uncertainties in the failure modeling of CFRP. It should be emphasized here that although the methodologies presented herein focus on adaptive composite marine propellers, the framework is also generally applicable to other flexible structures that undergo fluid–structure interactions, including wind or tidal turbines.

Acknowledgements

The authors are grateful to the Office of Naval Research (ONR) and Dr. Ki-Han Kim (program manager) for their financial support through grant numbers N00014-07-1-0491 and N00014-08-1-0475.

References

- [1] Khan AM. Flexible composite propeller design using constrained optimization techniques. Ph.D. thesis, Iowa State University; 1997.
- [2] Friedmann PP, Venkatesan C, Yuan K. Development of a structural optimization capability for the aeroelastic tailoring of composite rotor blades with straight and swept tips. In: 4th AIAA symposium on multidisciplinary analysis and optimization, Cleveland, OH; 1992.
- [3] Ganguli R, Chopra I. Aeroelastic optimization of a composite helicopter rotor. In: 4th AIAA symposium on multidisciplinary analysis and optimization, Cleveland, OH; 1992.

- [4] Ganguli R, Chopra I. Aeroelastic tailoring of composite couplings and blade geometry of a helicopter rotor using optimization methods. *J Am Helicopter Soc* 1997;42(3):218–28.
- [5] Soykasap O, Hodges DH. Performance enhancement of a composite tilt-rotor using aeroelastic tailoring. *J Aircraft* 2000;37:850–8.
- [6] Glaz B, Friedmann P, Lu L. Helicopter vibration reduction throughout the entire flight envelope using surrogate-based optimization. *J Am Helicopter Soc* 2009;54(1).
- [7] Yang Y. Structural analysis and multidisciplinary design of flexible fluid loaded composite canard. Ph.D. thesis, Iowa State University; 2005.
- [8] Lee AT, Flay RGJ. Compliant blades for passive power control of wind turbines. *Wind Eng* 2000;24:3–11.
- [9] Lobitz DW, Veers PS, Eisler GR, Laino DJ, Migliore PG, Bir G. The use of twist-coupled blades to enhance the performance of horizontal axis wind turbines. Tech rep, Sandia National Laboratories; 2000.
- [10] Lobitz DW, Veers PS. Load mitigation with bending/twist-coupled blades on rotors using modern control strategies. *Wind Energy* 2003;6:105–17.
- [11] Gowing S, Coffin P, Dai C. Hydrofoil cavitation improvements with elastically coupled composite materials. In: Proceedings of 25th American towing tank conference, Iowa City, IA; 1998.
- [12] Lee Y, Lin C. Optimized design of composite propeller. *Mech Adv Mater Struct* 2004;11:17–30.
- [13] Lin C, Lee Y. Stacking sequence optimization of laminated composite structures using genetic algorithm with local improvement. *Compos Struct* 2004;63:339–45.
- [14] Young YL, Michael TJ, Seaver M, Trickey ST. Numerical and experimental investigations of composite marine propellers. In: 26th symposium on naval hydrodynamics, Rome, Italy; 2006.
- [15] Young YL, Liu Z. Hydroelastic tailoring of composite naval propulsors. In: 26th International conference on offshore mechanics and arctic engineering, San Diego, CA; 2007.
- [16] Young YL. Fluid–structure interaction analysis of flexible composite marine propellers. *J Fluid Struct* 2008;24:799–818.
- [17] Motley MR, Liu Z, Young YL. Utilizing fluid–structure interactions to improve energy efficiency of composite marine propellers in spatially varying wake. *Compos Struct* 2009;90(3):304–13.
- [18] Chen B, Neely S, Michael T, Gowing S, Szwerc R, Buchler D, et al. Design, fabrication and testing of pitch-adapting (flexible) composite propellers. In: The SNAME propeller/shafting symposium, Williamsburg, VA; 2006.
- [19] Nicholls-Lee RF, Turnock SR. Enhancing performance of a horizontal axis tidal turbine using adaptive blades. In: OCEANS 2007 – Europe, Aberdeen, Scotland; 2007.
- [20] Frangopol DM, Maute K. Reliability-based optimization of civil and aerospace systems. *Engineering design reliability handbook*. CRC Press; 2005. 24–1–24–32 [chapter 24].
- [21] Allen M, Maute K. Reliability-based shape optimization of structures undergoing fluid–structure interaction phenomena. *Comput Method Appl M* 2005;194:3472–95.
- [22] Chamis CC. Design of smart composite structures in the presence of uncertainties. *J Chin Inst Eng* 2004;27:771–81.
- [23] Lekou DJ, Philippidis TP. Mechanical property variability in FRP laminates and its effect on failure prediction. *Compos Part B Eng* 2008;39:1256–74.
- [24] Rais-Rohani M, Singh MN. Comparison of global and local response surface techniques in reliability-based optimization of composite structures. *Struct Multidiscip O* 2004;26:333–45.
- [25] Young YL. Time-dependent hydroelastic analysis of cavitating propulsors. *J Fluid Struct* 2007;23:269–95.
- [26] Huang TT, Groves NC. Effective wake: theory and experiment. Tech rep, David Taylor Naval Ship Research and Development Center, Bethesda, MD; 1981.
- [27] Choi JK, Kinnas SA. Prediction of non-axisymmetric effective wake by a three-dimensional Euler solver. *J Ship Res* 2001;45:13–33.
- [28] ABAQUS. ABAQUS version 6.5 documentation. ABAQUS, Inc.; 2005.
- [29] Young YL, Liu Z, Motley MR. Influence of material anisotropy on the hydroelastic behaviors of composite marine propellers. In: Proceedings of the 27th symposium on naval hydrodynamics, Seoul, Korea; 2008.
- [30] Plucinski M, Young YL, Liu Z. Optimization of a self-twisting composite marine propeller using a genetic algorithm. In: Proceedings of 16th international conference on composite materials, Kyoto, Japan; 2007.
- [31] Melchers RE. Structural reliability analysis and prediction. 2nd ed. Chichester (NY): John Wiley; 1999.